Journal of Power Sources 253 (2014) 138–142

Contents lists available at ScienceDirect

Journal of Power Sources

journal homepage: www.elsevier.com/locate/jpowsour

Short communication

Theoretical study on $Sm_xSr_{1-x}MnO_3$ as a potential solid oxide fuel cell cathode

Lichao Jia [a], Xin Wang [a], Wenlu Li [a], Kai Li [a], Bo Chi [a], Jian Pu [a], Li Jian [a,*], Songliu Yuan [b]

[a] School of Materials Science and Engineering, State Key Lab of Material Processing and Die & Mould Technology, Huazhong University of Science and Technology, Wuhan, Hubei 430074, China
[b] School of Physics, Huazhong University of Science and Technology, Wuhan, Hubei 430074, China

HIGHLIGHTS

- SSM50 has better oxygen storage capacity than LSM50.
- The absorbed O_2 species on SSM50 (100) surface are readily dissociated.
- SSM50 has the best catalysis for the ORR among the considered systems.

ARTICLE INFO

Article history:
Received 20 May 2013
Received in revised form
29 October 2013
Accepted 31 October 2013
Available online 1 December 2013

Keywords:
Cathode
First principle
Oxygen reduction
Diffusion

ABSTRACT

Cubic perovskite $Sm_xSr_{1-x}MnO_3$ (SSM) surface and bulk models have been constructed to simulate the oxygen reduction reactions by employing first-principles calculations. The results demonstrate that oxygen vacancies can be formed easily in $Sm_{0.5}Sr_{0.5}MnO_3$ (SSM50). The oxygen migration barrier in bulk SSM50, which is predicted by the nudged elastic band (NEB) method, is the lowest, while the adsorption energy of O_2 molecular on SSM50 (100) surface is the lowest among the considered doping systems, indicating the potential application of SSM50 as a cathode for intermediate-temperature solid oxide fuel cell (IT-SOFC). The reaction mechanisms of oxygen reduction on SSM50 (100) surface have also been studied.

© 2013 Elsevier B.V. All rights reserved.

1. Introduction

Solid oxide fuel cell (SOFC) has received increasing attention in recent decades because it has higher efficiency and lower pollutant emission compared with other conventional energy conversion devices [1–3]. Lanthanum strontium manganite (LSM) is the most conventional cathode for high temperature SOFC [4–6]. However, with the decrease of operating temperature, the polarization resistance increases significantly [7], which limits the application of the LSM based cathodes for intermediate-temperature SOFC (IT-SOFC). The polarization resistance of the cathode originates from the oxygen reduction reaction (ORR) [8]. The oxygen adsorption on the cathode surface and the oxygen vacancy migration in the cathode are the crucial factors which affect the polarization resistance during the ORR [9]. These two factors can be characterized by oxygen adsorption energy and ionic diffusion activation energy, respectively.

Great efforts [10–13] have been made to study the mechanism of ORR and develop SOFC cathodes with good performance. Among these studies, Density Functional Theory (DFT) calculation has become an important and powerful tool which allows us to gain further insight into the nature of the oxygen exchange reaction. Oxygen adsorption and diffusion in the common used LSM cathode have been studied systemically by Kuklja [13]. It is found that the ORR mainly occurs on the MnO_2-terminated surface and the surface migration of the adsorbed O species is slower than that of surface O vacancies. Liu et al. [8,14,15] have examined the electrochemical reaction activities of cathode with different perovskite-type materials such as $Pr_xSr_{1-x}MnO_3$, $Nd_xSr_{1-x}MnO_3$, $Pm_xSr_{1-x}MnO_3$, and $Sm_xSr_{1-x}MnO_3$ (SSM). It is found that only (SSM) exhibits superior electrochemical performance [14]. SSM is an electronic conductor, but it can become a mixed ionic-electronic conductor (MIEC) under cathodic polarization because polarization promotes an in-situ electrochemical reduction of the Mn^{4+} in SSM

* Corresponding author. Tel.: +86 27 87557694; fax: +86 27 87558142.
E-mail address: lijian@hust.edu.cn (L. Jian).

0378-7753/$ – see front matter © 2013 Elsevier B.V. All rights reserved.
http://dx.doi.org/10.1016/j.jpowsour.2013.10.146

to Mn^{3+} with the introduction of oxygen vacancies into SSM. The previous work only considered the case of $x = 0.5$, and there has been no discussion on the mechanism of oxygen reduction. Therefore, the DFT calculations on the complex SSM are conducted in the present work. Besides, the formation of bulk oxygen vacancies and their diffusions, as well as the oxygen adsorption property on the SSM surface are studied.

2. Computational

The *ab initio* DFT computer code VASP [16,17], which uses the plane-wave pseudopotential total energy calculation method [18], is introduced to conduct all the first-principles calculations. The exchange correlation of electrons is parameterized by Perdew–Burke–Ernzerhof (PBE) [19] formula within the generalized gradient approximation (GGA). The Brillouin zone sampling $4 \times 4 \times 4$ Monkhorst–Pack k-points [20] for bulk and $2 \times 3 \times 1$ for surface is adopted, and the cutoff energy is set to be 400 eV, according to the result of convergence test. Using the block Davidson scheme, both the atomic positions and cell parameters are optimized until the residual force is below 0.01 eV $Å^{-1}$. Since the $LaMnO_3$-based cathode material has a cubic structure under SOFC operating conditions [15,21], and $SrMnO_3$ also has a cubic structure at high temperatures, we first constructed an ideal cubic perovskite structure of $SrMnO_3$ (space group $Pm\bar{3}m$). The calculated lattice parameter after structure optimization is 3.802 Å, which is in good agreement with the experimental values of 3.805 Å [22]. When part of or all the Sr atoms have been replaced by Sm atoms, there are only tiny changes of the lattice parameter but the structures remain cubic. Based on the above results, it is assumed that SSM cathode also has a cubic perovskite structure in our calculations. Therefore, only the highly symmetric cubic perovskite structure is considered similar to previous study [14]. All the doped systems are constructed from a relaxed $(2 \times 2 \times 1)$ $SrMnO_3$ supercell, with Sm doping in SSM at $x = 0, 0.25, 0.5, 0.75, 1$, respectively. In the calculation, the 4f electrons of Sm are treated as core electrons, and the electronic configurations are considered, included Sm ($5s^2 5p^6 5d^1 6s^2$), Sr ($4s^2 4p^6 5s^2$), Mn ($3d^5 4s^2$), and O ($2s^2 2p^4$).

3. Results and discussion

3.1. Bulk diffusion of O vacancy

A good SOFC cathode should be a good MIEC. The bulk diffusion of O vacancy in SSM is studied in the first. The diffusion activation energy E_a is applied to characterize the difficulty of an oxygen ion (or vacancy) migration in bulk SSM. According to Liu et al. [13], the E_a is divided into two parts: the oxygen-vacancy formation energy (E_{vac}), and the migration barrier (E_m) of the oxygen ion (or vacancy). And they are described as

$$E_a + E_{vac} + E_m. \quad (1)$$

An O vacancy is introduced into the SSM $(2 \times 2 \times 1)$ supercell, forming a defect structure of $Sm_xSr_{1-x}MnO_{2.75}$. The corresponding oxygen-vacancy formation energy can be calculated by

$$E_{vac} = E_{Sm_xSr_{1-x}MnO_{2.75}} + \frac{1}{2}E_{O_2} - E_{Sm_xSr_{1-x}MnO_3}, \quad (2)$$

where $E_{Sm_xSr_{1-x}MnO_{2.75}}$ and $E_{Sm_xSr_{1-x}MnO_3}$ represent the total energies of bulk SSM with and without an oxygen vacancy, respectively. The total energy of O_2 (E_{O_2}) is calculated in a 9 Å × 10 Å × 11 Å box, to prevent the effect of the degeneracy. After geometry optimization, all the reduced structures show distortions around the vacancy site. The calculated E_{vac} are listed in Table 1. It is found that the oxygen-vacancy formation energy depends strongly on the dopant concentration. As we can see, E_{vac} becomes smaller as the Sm doping concentration increases. When half of the Sr atoms are replaced by Sm, the value of E_{vac} is 2.58 eV, which is smaller than that of $La_{0.5}Sr_{0.5}MnO_3$ (LSM50) (3.25 eV) [14], indicating the oxygen vacancies can be formed more easily in SSM50 than in LSM50. In other words, SSM50 has better oxygen storage capacity than LSM50.

Table 1
Calculated energies for oxygen-vacancy formation E_{vac} and the migration barriers (E_m) in varies bulk SSM.

SSM	E_{vac} (eV)	E_m (eV)	E_a (eV)
$SrMnO_3$	1.52	0.73	2.25
$Sm_{0.25}Sr_{0.75}MnO_3$	2.30	0.85	3.15
$Sm_{0.5}Sr_{0.5}MnO_3$	2.58	0.75	3.33
$Sm_{0.75}Sr_{0.25}MnO_3$	3.40	0.96	4.36
$SmMnO_3$	3.75	1.02	4.77

To predict the migration barrier of an oxygen ion in $Sm_xSr_{1-x}MnO_{2.75}$, we assume that the oxygen ion is diffused directly to its neighbor vacancy site, as shown in Fig. 1. Under this assumption, a migrating oxygen ion has to pass through the triangular orifice consisting of two large Sr (or Sm) and one small Mn atoms in the crystal lattice. We first find out the transition states using the nudged elastic band (NEB) method [23,24]. The energy difference between Transition State (TS) and the Initial State (IS) represents the migration barrier. The migration barriers in various SSM systems are shown in Table 1, together with the corresponding activation energy. It can be concluded that the oxygen ion overcomes a barrier of 0.75 eV when migrating to its neighbor site in SSM50. The same as the case of other cathode materials, e.g. (Ba, Sr)(Co, Fe)O_3 [25], the value of the migration barriers varies with the different doping concentration.

According to the Equation (1), the diffusion activation energy E_a is the sum of E_{vac} and E_m. According to Table 1, the E_a of SSM50 is 3.33 eV, a little bit higher than that of $SrMnO_3$ and $Sm_{0.25}Sr_{0.75}MnO_3$. However, because the valence of Sr is +2 in SSM50, which is lower than that of Sm (+3), half of the Mn^{3+} ions will change to Mn^{4+} for the balance of the charge. The coexistence of Mn^{3+} and Mn^{4+} will form an electronic transmission channel (Mn^{3+}–O–Mn^{4+}), which can lead to a better electronic conductivity [26] for SSM50 than $SrMnO_3$ and $Sm_{0.25}Sr_{0.75}MnO_3$ (SSM50 has more conducting electrons than $Sm_{0.25}Sr_{0.75}MnO_3$ does). Based on the above considerations, SSM50 is most suitable as SOFC cathode among the considering systems.

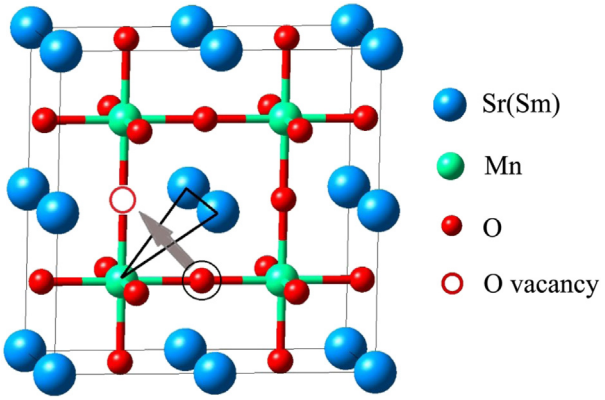

Fig. 1. Schematic representations of oxygen ion migration in defect bulk SSM.

3.2. Surface adsorption and diffusion

The oxygen adsorption at the cathode surface is a critical step during the cathode oxygen reduction process. In order to study the adsorption characteristics, we model the O_2 (and O) adsorption on the SSM (100) surface, since it is energetically the most stable surface among the low-index (100), (110), and (111) surfaces. The SSM (100) surface consists of alternating MnO_2 and Sr(Sm)O plane. According to the results of convergence test, a six-layer slab is thick enough to simulate the adsorption. Supercells with periodicity (2×1) are employed to reduce the influence of the interaction between the adsorbed species, and the periodically repeated slabs are separated by a 15 Å thick vacuum layers to avoid the interaction between the two surfaces. Fig. 2 shows the side elevation of O_2 adsorption on SSM (100) surface. All of the six layers are allowed to be relaxed during the geometry optimization.

The adsorption energy (E_{ads}), which corresponds to the energy gained from the adsorption process, is defined by

$$E_{ads} = E_{adsorbate+slab} - E_{slab} - E_{adsorbate},$$

where $E_{adsorbate+slab}$ is the total energy of the adsorbed assembly, E_{slab} and $E_{adsorbate}$ are the energies of the clean surface and the adsorbate, respectively. The value of E_{ads} is a criterion to determine the difficulty and stability of the adsorption. The more negative the E_{ads} is, the easier and the more stable the adsorbate can be adsorbed on the surface. Previous study [13,27] shows that B cations are more active than A cations for oxygen reduction on several perovskite-type ABO_3 cathodes. Only the outermost Mn atoms (atop Mn) on the MnO_2-terminated surface are considered in this study.

The calculated adsorption energy and structural parameters for O_2 adsorption on the atop Mn of SSM (100) surfaces are summarized in Table 2. The calculated bond length of O_2 molecule in equilibrium gas phase is 1.234 Å, slightly larger than experimental value of 1.210 Å. When adsorbed on the SSM surface, the bond lengths of the O_2 molecule increase to 1.275–1.285 Å. The increase of the bond length designates that the absorbed O_2 species are readily to be dissociated. The distance between O1 and the surface Mn ranges from 1.728 Å to 1.773 Å, which are smaller than the sum of the radius of Mn^{3+}/Mn^{4+} and O^{2-}, demonstrating that Mn and O are connected by chemical bond.

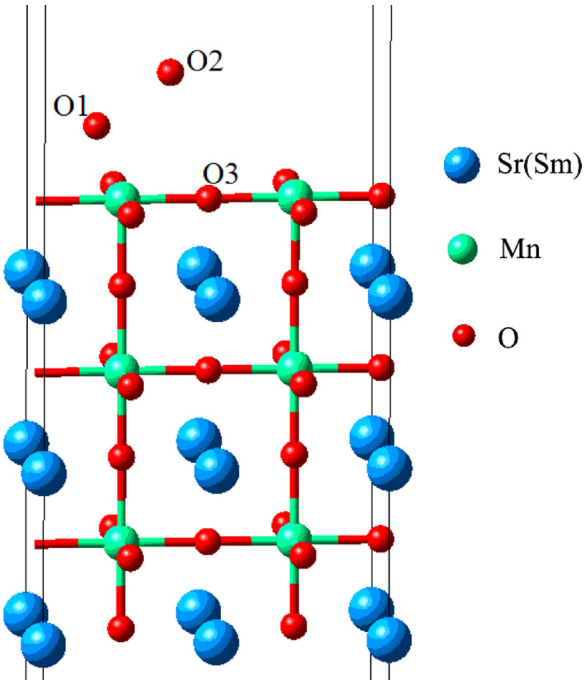

Fig. 2. The side elevation of O_2 adsorption on SSM (100) surface.

Table 2
Calculated adsorption energy (E_{ads}) and structural parameters[a] for O_2(O) adsorption on the atop surface Mn atoms of SSM (100) surfaces.

	O_2				O	
	E_{ads} (eV)	d_{O1-Mn} (Å)	d_{O1-O2} (Å)	E_{diss} (eV)	E_{ads} (eV)	d_{O1-Mn} (Å)
$SrMnO_3$	−3.09	1.773	1.275	0.62	−2.49	1.589
$Sm_{0.25}Sr_{0.75}MnO_3$	−3.13	1.741	1.281	0.70	−2.78	1.591
$Sm_{0.5}Sr_{0.5}MnO_3$	−3.94	1.737	1.285	0.53	−3.35	1.591
$Sm_{0.75}Sr_{0.25}MnO_3$	−3.93	1.728	1.281	0.59	−3.39	1.592
$SmMnO_3$	−3.52	1.730	1.283	0.74	−3.25	1.587

d_{O1-Mn}: distance between O1 and the nearest Mn atom. d_{O1-O2}: distance between O1 and O2.
[a] O1 atom nearest to the surface, O2 atom far from the surface (as shown in Fig. 1).

Besides the adsorption energy, the O_2 dissociation energy is also one of key parameters that need to be discussed. Using the same method described by Mastrikov [28], the dissociation energies (E_{diss}) of the adsorbed O2 have been calculated and listed in Table 2. The E_{diss} ranges from to 0.53–0.74 eV, indicating that the adsorbed O_2 can be easily dissociated.

In SSM50 system, the E_{ads} and E_{diss} of O_2 molecular are calculated to be −3.94 V and 0.53 eV, lower compared to that of any other systems; and the bond length of the adsorbed O_2 is larger than that of the other systems too, implying that SSM50 may have the best catalysis for the ORR among these five systems. Along with the O_2 molecule adsorption, the adsorption properties for O atom on the SSM (100) surfaces are calculated. The result shows a strong preference for O atom adsorption on the SSM50 (100) surface.

Previous study [28] demonstrates that surface vacancy diffusion energy (E_{diff}) strongly differs from that in the bulk. Thus, the E_{diff} also has been calculated (Table 3) using the NEB method. The same as the diffusion in the bulk SSM, we assume that the oxygen ion is diffused directly to its neighbor vacancy site (Fig. 3). It is found that E_{diff} is higher than the relevant E_m, clarifying that it is surface diffusion that is limiting the overall oxygen vacancy diffusion rate.

Combining the oxygen-vacancy formation energy, the migration barrier, the adsorption and dissociation energy, as shown in Tables 1 and 2, we can conclude that SSM50 is a potential SOFC cathode material with excellent performance for ORR.

3.3. PDOS analysis of the adsorbed assemblies

To explore the deep mechanism of the interaction between the adsorbates and surfaces, partial densities of states (PDOS) calculations on the O_2 molecular adsorbed SSM50 (100) surface are carried out. The 2*p* orbitals of the adsorbed O atoms and the surface O

Table 3
Calculated oxygen vacancy diffusion energy (E_{diff}) on SSM (100) surface.

System	$SrMnO_3$	$Sm_{0.25}Sr_{0.75}MnO_3$	$Sm_{0.5}Sr_{0.5}MnO_3$	$Sm_{0.75}Sr_{0.25}MnO_3$	$SmMnO_3$
E_{diff} (eV)	0.86	0.95	0.97	1.02	1.08

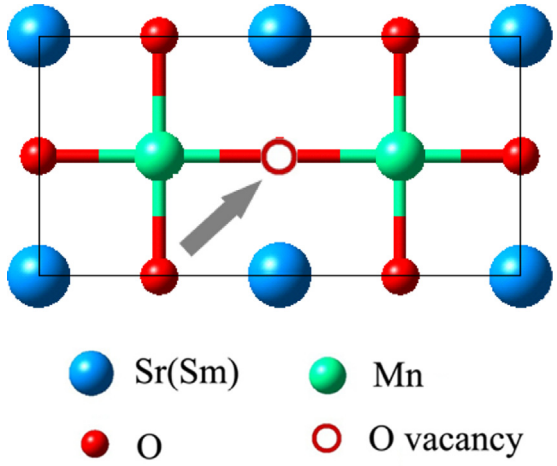

Fig. 3. Top view of the oxygen ion diffusion on SSM (100) surface.

atoms, as well as the 3*d* states of the relative Mn atom before and after adsorption are shown in Fig. 4. For the surface without O_2 adsorption (see Fig. 4(a)), it is found that Mn 3*d* orbitals exhibits broad bands very close to the Fermi level, indicating a strong itinerancy of Mn 3*d* electrons [29], thus the Mn^{4+} ions can easily transform into Mn^{3+}. There is an overlap between Mn 3*d* orbitals and the 2*p* orbitals of the adjacent surface O atom (O3) in the range of −6 to 3 eV. This is in contrast with the DOS for other typical perovskites with large band gap [25]. And the overlap reveals that Mn and O atoms are held together by Mn–O chemical bond. After adsorption, as shown in Fig. 4(b), Mn 3*d* electrons transfer to lower energy level and hybridized with the 2*p* electrons of the adsorbed O atoms. The hybridization between O 2*p* states and Mn 3*d* states is quite strong around the energy level of −1.0 eV. The splitting and broadening of peaks indicate a strong interaction between Mn and the adsorbed O atom, which facilitate the adsorption of O_2 on the atom Mn of SSM50 surface. The overlap between the 2*p* states of O1 and O2 at around −1.0 eV, −6.8 eV and −7.9 eV reveals that O1 and O2 are still bonded together. It can be seen from Fig. 2 that the adsorbed O atom, which is far from the Mn atom (O2) has an inclination to bond together with O3. Thus, the 2*p* states of O2 and O3 are also sketched in Fig. 4(b). There is a peak formed by the 2*p* states of O3 at about −6.6 eV. This can be attributed to the interaction between O2 and O3. The formation of O2–O3 bond contributes much to the dissociation of the adsorbed O_2 molecule.

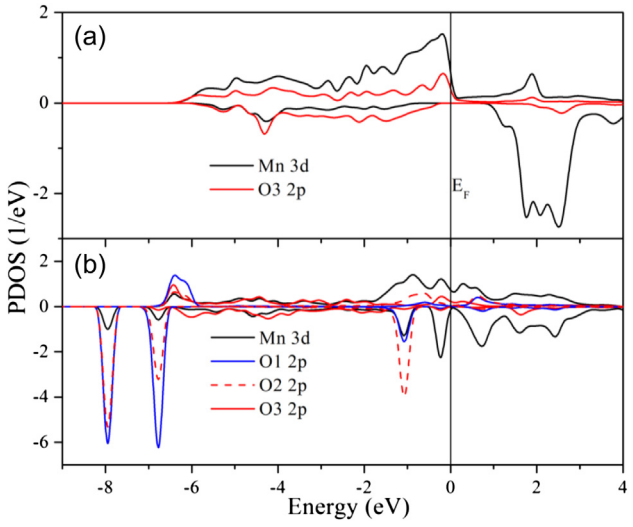

Fig. 4. Calculated PDOS of Mn and O before and after O_2 adsorption on SSM50 (100) surface. The Fermi level is set to be 0.

4. Conclusions

In summary, the first-principles density functional theory calculations were performed to investigate the SSM cathodic reaction process: bulk diffusion and surface adsorption. It can be concluded that SSM50 is a potential cathode material applying for IT-SOFC. The obtained results are as follows:

(1) The oxygen-vacancy formation energy of SSM depends strongly on the dopant concentration. The formation of an oxygen vacancy in SSM50 needs an energy of 2.58 eV; it is easier than the formation in LSM50.
(2) The oxygen migration barrier in bulk SSM50 is 0.75 eV. The corresponding diffusion activation energy shows that SSM50 is the most suitable cathode material among these systems considered.
(3) The O_2 molecular can be adsorbed on the SSM50 (100) surface easily, with an adsorption energy of −3.94 eV. The predicted bond length of O_2 molecule after adsorption indicates that the absorbed O_2 species can be readily dissociated and the dissociation energy is determined to be 0.53 eV.

Acknowledgments

This research was financially supported by National Natural Science Foundation of China (U1134001), National 863 project of China (2011AA050702) and China Postdoctoral Science Foundation (2012M521423).

References

[1] B.C.H. Steele, A. Heinzel, Nature 414 (2001) 345–352.
[2] S.C. Singhal, K. Kendall, High-temperature Solid Oxide Fuel Cells: Fundamentals, Design and Applications, Elsevier Science, 2003.
[3] S.C. Singhal, Solid State Ionics 135 (2000) 305–313.
[4] S.P. Jiang, Y.J. Leng, S.H. Chan, K.A. Khor, Electrochem. Solid State Lett. 6 (2003) A67–A70.
[5] C.W. Sun, R. Hui, J. Roller, J Solid State Electrochem. 14 (2010) 1125–1144.
[6] K. Katsiev, B. Yildiz, K. Balasubramaniam, P.A. Salvador, Appl. Phys. Lett. 95 (2009) 092106.
[7] C.R. Xia, M.L. Liu, Adv. Mater. 14 (2002) 521–523.
[8] Y.M. Choi, M.E. Lynch, M.C. Lin, M.L. Liu, J. Phys. Chem. C 113 (2009) 7290–7297.
[9] M.L. Liu, M.E. Lynch, K. Blinn, F. Alamgir, Y.M. Choi, Mater. Today 14 (2011) 534–546.
[10] S.P. Simner, J.R. Bonnett, N.L. Canfield, K.D. Meinhardt, J.P. Shelton, V.L. Sprenkle, J.W. Stevenson, J. Power Sources 113 (2003) 1–10.
[11] J. Chen, F.L. Liang, D. Yan, J. Pu, B. Chi, S.P. Jiang, J. Li, J. Power Sources 195 (2010) 5201–5205.
[12] F.L. Liang, J. Chen, Bo Chi, J. Pu, S.P. Jiang, J. Li, J. Power Sources 196 (2011) 153–158.
[13] M.M. Kuklja, E.A. Kotomin, R. Merkle, Yu. A. Mastrikova, J. Maier, Phys. Chem. Chem. Phys. 15 (2013) 5443–5471.
[14] Y.M. Choi, M.C. Lin, M.L. Liu, J. Power Sources 195 (2010) 1441–1445.
[15] Y.M. Choi, D.S. Mebane, M.C. Lin, M.L. Liu, Chem. Mater. 19 (2007) 1690–1699.
[16] G. Kresse, J. Furthmüller, Phys. Rev. B 54 (1996) 11169–11186.
[17] G. Kresse, J. Hafner, Phys. Rev. B 49 (1994) 14251–14269.
[18] P.E. Blöchl, Phys. Rev. B 50 (1994) 17953–17979.
[19] J.P. Perdew, K. Burke, M. Ernzerhof, Phys. Rev. Lett. 77 (1996) 3865–3868.
[20] H.J. Monkhorst, J.D. Pack, Phys. Rev. B 13 (1976) 5188–5192.
[21] R.A. Evarestov, E.A. Kotomin, Y.A. Mastrikov, D. Gryaznov, E. Heifets, J. Maier, Phys. Rev. B 72 (2005), 214411/1.
[22] O. Chmaissem, B. Dabrovski, S. Kolesnik, J. Mais, D.E. Brown, R. Kruk, P. Prior, B. Pyles, J.D. Jorgensen, Phys. Rev. B 64 (2001) 134412.
[23] G. Mills, H. Jönsson, G. Schenter, Surf. Sci. 324 (1995) 305–337.
[24] G. Henkelman, B.P. Uberuaga, H. Jönsson, J. Chem. Phys. 113 (2000) 9901–9904.

[25] R. Merkle, Y.A. Mastrikov, E.A. Kotomin, M.M. Kuklja, J. Maier, J. Electrochem. Soc. 159 (2012) B219–B226.
[26] Z.C. Xia, C.Q. Tang, Acta Phys. Sin. Chin. Ed. 48 (1999) 1518–1522.
[27] Y.J. Zhou, Z. Lü, B. Wei, X.B. Zhu, X.Q. Huang, W. Jiang, W.H. Su, J. Power Sources 209 (2012) 158–162.
[28] Y.A. Mastrikov, R. Merkle, E. Heifets, E.A. Kotomin, J. Maier, J. Phys. Chem. C 114 (2010) 3017–3027.
[29] L.C. Jia, X. Wang, B. Hua, W.L. Li, B. Chi, J. Pu, J. Li, Int. J. Hydrogen Energy 37 (2012) 11941–11945.